

Development of iron-based nanoparticles for Cr(VI) removal from drinking water

K. Simeonidis¹, M. Tziomaki¹, M. Angelakeris², C. Martinez-Boubeta³, Ll. Balcells⁴, C. Monty⁵, M. Mitrakas⁶, G. Vourlias², N. Andritsos¹

¹Department of Mechanical Engineering, School of Engineering, University of Thessaly, 38334 Volos, Greece

²Department of Physics, Aristotle University of Thessaloniki, 54124 Thessaloniki, Greece

³Departament d'Electrònica, MIND-IN2UB, Universitat de Barcelona, 08028 Barcelona, Spain

⁴Institut de Ciència de Materials de Barcelona, Campus Universitat Autònoma de Barcelona, 08193 Bellaterra, Spain

⁵Procédés, Matériaux et Energie Solaire, Centre National de la Recherche Scientifique, Odeillo, 66120 Font-Romeu, France

⁶Analytical Chemistry Laboratory, Department of Chemical Engineering, Aristotle University of Thessaloniki, 54124 Thessaloniki, Greece

Abstract. A great deal of research over recent decades has been motivated by the requirement to lower the concentration of chromium in drinking water. This study has been conducted to determine the feasibility of iron-based nanoparticles for chromium removal from contaminated water. Single Fe, Fe₃O₄ and binary Fe/Fe₃O₄ nanoparticles were grown at the 45-80 nm size range using the solar physical vapor deposition technique and tested as potential hexavalent chromium removing agents from aqueous solutions. Due to their higher electron donation ability compared to the Fe₃O₄ ones, single Fe nanoparticles exhibited the highest Cr(VI) removal capacity of more than 3 µg/mg while maintaining a residual concentration 50 µg/L, equal to the regulation limit for drinking water. In combination to their facile and fast magnetic separation, the applicability of the studied particles in water treatment facilities should be considered.

1 Introduction

Among the uses of magnetic nanoparticles in a variety of application fields, their incorporation in traditional environmental and health safety treatment methods is gradually earning much interest [1]. Their ability to sufficiently remove heavy metals or other pollutants from drinking or waste water accompanied by the possibility of magnetically controlling their dispersion may introduce additional opportunities for increasing the yield and reducing the cost of such processes.

However, depending on the contaminant, its concentration levels and the relevant regulation, the required physical properties of nanoparticles may significantly vary. For instance, most of the reported studies for the removal of arsenic, lead, chromate and other heavy metals appear very efficient in terms of percentage reduction at relatively high concentrations [2] but only few of them provide reasonable results complying with the regulations for drinking water safety when tested at reliable concentrations met in natural water [3]. Therefore, in order to decide and prepare the proper magnetic nanoparticle system for each case, specialized approaches should be designated and carried out considering parameters like the mechanism of

contaminant capture, their affinity, the kinetic rate of the process and the effect of interfering factors usually existing during application.

The presence of chromate ions, also referred to as hexavalent chromium Cr(VI), in groundwater has only recently been discussed as an important issue related to drinking water in many regions worldwide due to the indications for harmful effects on human health upon regular consumption [4]. Since the existing tolerance limit in potable water corresponding to total chromium (50 µg/L) [5] practically underestimates the health risks, the establishment of a separate and very strict limit for the Cr(VI) form is anticipated soon. Thus, the development of optimized low-cost methods for its treatment is essential. In practice, Cr(VI) is usually removed from water either by chemical coagulation/filtration, ion exchange, reverse osmosis or adsorption [6]. The experience from other contaminants (e.g. arsenic) indicates that the adsorption process, providing high efficiency and environmentally safe disposal, is the simplest and one of the cheapest methods. Moreover, the use of consumable adsorbents in the case of Cr(VI) removal can be further facilitated by the incorporation of a Cr(VI) to Cr(III) reduction stage.

Considering this, the increased specific surface area

and surface reactivity of nanosized particles favor the enhancement of chromate reduction. In this work, zero-valent iron (ZVI) and magnetite (Fe_3O_4) nanoparticles, were prepared by solar physical vapor deposition (Solar PVD) and tested as potential Cr(VI) adsorbents capable of reducing Cr(VI) and subsequently immobilize the resulting Cr(III) within their surface.

2 Experimental

2.1 Preparation of nanoparticles

The studied Fe, Fe_3O_4 and Fe/ Fe_3O_4 nanoparticles were synthesized by using the solar physical vapor deposition technique under inert argon atmosphere [7]. In this process, the target material is placed in the focus of a 2 kW solar concentrator and the fume produced by evaporation is condensed on a cold finger or trapped on a nanoporous ceramic filter (Figure 1). The nanoparticles are then collected by brushing. The arrangement is constituted of a “heliostat” which tracks the sun and reflects the radiation on a parabolic concentrator mirror (diameter 2 m). The particles size and the growth rate can be controlled with the gas pressure and the power supplied which is controlled by a flag located between the concentrator and the heliostat. The targets used for nanoparticles production were cold-pressed pellets prepared by Fe and/or Fe_3O_4 powders purchased from Alfa Aesar (>99 %). In the studied samples, the chamber’s dynamic pressure was set to 80 Torr by introducing an argon flow.

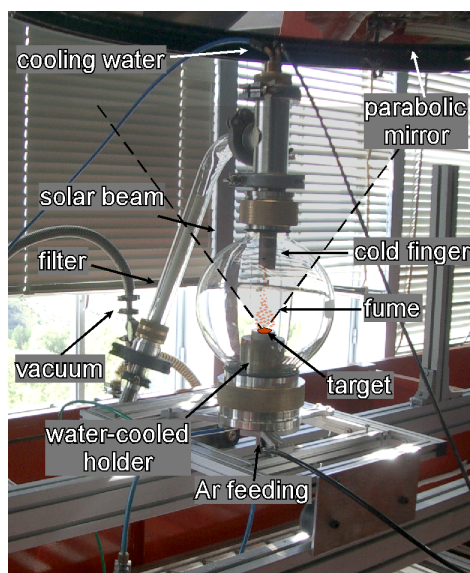


Fig. 1. Solar physical vapor deposition apparatus for the growth of nanoparticles.

2.2 Characterization

The crystal structure of the nanoparticles was determined using transmission electron microscopy (TEM) and X-ray diffraction (XRD). For the TEM analysis, a drop of the colloidal solution in water was deposited onto a thin carbon film supported by a 400 mesh copper grid.

Measurements were carried out with a JEOL 100Cx TEM microscope working at an acceleration voltage of 100 kV. XRD patterns were taken with a Rigaku Ultima+ powder diffractometer using $\text{Cu-K}\alpha$ radiation. Magnetic characterization of the nanoparticles by vibrating sample magnetometry (VSM) provided the necessary information for the possibility of their magnetic recovery from an aqueous dispersion. Hysteresis loops at room temperature were recorded using an Oxford Instruments 1.2H/CF/HT VSM. In addition, magnetic separation experiments were performed by counting the rate of particles recovery from a suspension when applying a 15 T/m external field by means of permanent magnets in the sides of a 20 mL test tube. Chemical analysis of the nanoparticles was performed via graphite furnace atomic absorption spectrophotometry (Perkin Elmer Analyst 800) after diluting a weighted quantity in HCl. Similarly, residual iron concentrations dissolved after chromate removal were measured.

2.3 Chromate removal

The applicability of the nanoparticles as Cr(VI) adsorbents was evaluated by batch adsorption tests. Experiments were held by adding a quantity of nanoparticles (100-200 mg/L) in a volume of Cr(VI)-containing distilled water (250-1000 μg Cr(VI)/L) and shaking for a sufficient period of time (24 h) at room temperature. The equilibrium pH was adjusted to 7. Determination of the residual chromate was performed by the diphenylcarbazide spectrophotometric method while total chromium concentration was comparatively measured by graphite furnace atomic absorption spectrophotometry. The plotted isotherms represent the variation of Cr(VI) uptake per particles mass as a function of residual Cr(VI) fitted by a Langmuir function.

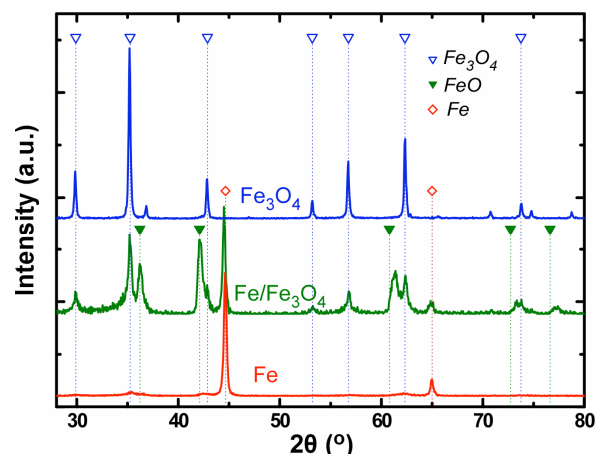


Fig. 2. XRD diagrams of Fe, Fe/ Fe_3O_4 and Fe_3O_4 nanoparticles.

3 Results

3.1. Morphology and structure

The identification of the samples’ crystal structure through XRD mostly indicated the preservation of the

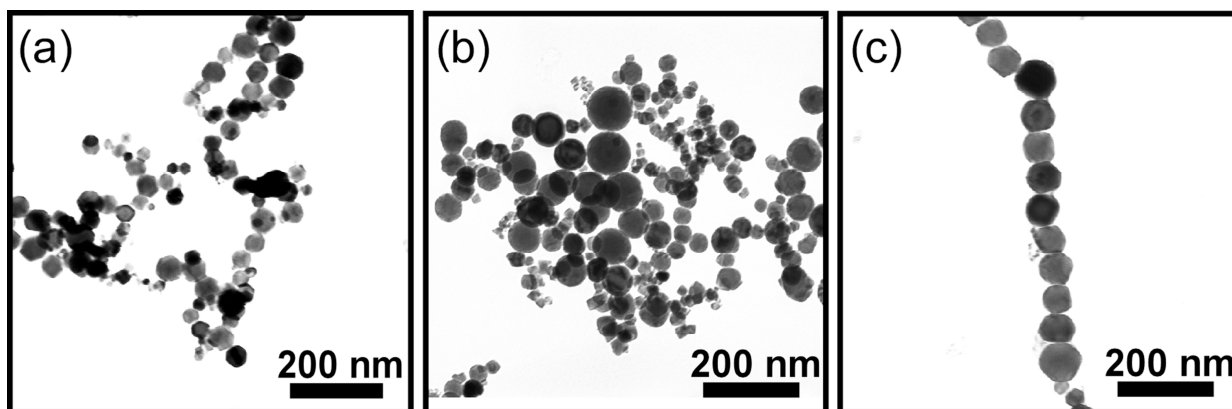


Fig.3. TEM images of Fe (a), Fe/Fe₃O₄ (b) and Fe₃O₄ (c) nanoparticles.

target's composition during evaporation/condensation whereas there is evidence for the surface oxidation of Fe (to FeO and Fe₃O₄) after exposure to the atmosphere (Figure 2). On the other hand, single magnetite nanoparticles are found to be very stable. The quantitative Rietveld analysis of the diagrams estimated the composition for single Fe nanoparticles 80 %wt Fe, 5 %wt FeO and 15 %wt Fe₃O₄ while the co-evaporation of Fe and Fe₃O₄ resulted in a mixture of nanoparticles with a total composition of 20 %wt Fe, 25 %wt FeO and 55 %wt Fe₃O₄.

The TEM observations for the samples are summarized in the images of Figure 3. Using Solar PVD for the growth of iron-based nanoparticles, a truncated-octahedral shape was always favored. It is important to note that single Fe₃O₄ particles formed long linear chains which indicate the effect of dipole-dipole magnetic interactions without serious agglomeration despite their relatively large diameter and the absence of surfactants. However, the mean diameter was different for Fe and Fe₃O₄ nanoparticles: iron nanoparticles were grown at an average size of 45 nm with a standard deviation around 15 % while Fe₃O₄ nanoparticles showed a diameter of 80 nm with a standard deviation around 10 %. Similar sizes for the two kinds of particles were met in the sample consisting of Fe/Fe₃O₄ particles being prepared by the co-evaporation of the two phases. The fraction of smaller Fe particles appears more susceptible to complete (Fe₃O₄) or partial (FeO) oxidation and thus should be responsible for the decrease of total metal iron content suggested by XRD analysis.

3.2 Magnetism

The response of the magnetic nanoparticles under a constant field is the major motivation for their application in water treatment. Therefore, the magnetic characterization may provide an estimation for the potential success of magnetophoresis. Figure 4 presents the hysteresis loops for the single and binary Fe and Fe₃O₄ nanoparticles. Samples showed relatively high saturation magnetization values approaching reference values for the corresponding bulk materials. The highest value was measured for the ZVI nanoparticles (200 emu/g) whereas Fe/Fe₃O₄ nanoparticles reached 86 emu/g and Fe₃O₄ 90 emu/g. In all the cases magnetization

mostly scales with the Fe and Fe₃O₄ content calculated by XRD refinement.

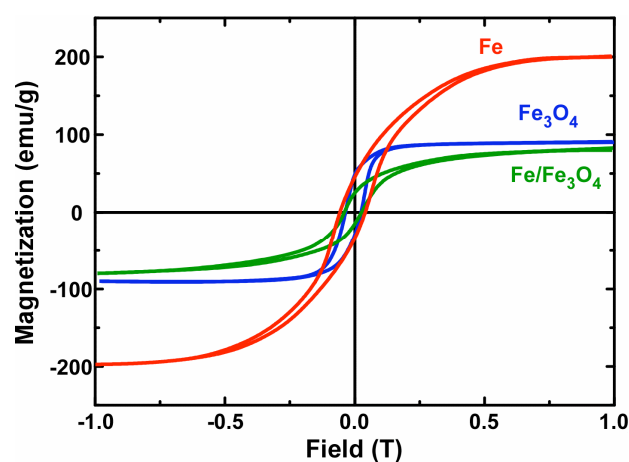


Fig. 4. Room temperature magnetic hysteresis loops of Fe, Fe/Fe₃O₄ and Fe₃O₄ nanoparticles.

According to saturation magnetization values and the geometrical characteristics of the nanoparticles, the minimum particle size that can be removed by the applied field of 15 T/m could be estimated by setting the applied magnetic force equal to the Brownian forces in the dispersion [8]. Such calculation assumes the absence of interactions between the nanoparticles. The solution gives e.g. a critical diameter of 140 nm for the sample mainly consisting of zero valent iron, indicating that separation of the 45 nm particles is not feasible. However, the preliminary experiments using dispersion of 100 mg/L, showed not only the complete but also the fast separation in all the samples. In particular, the time of observed separation for the Fe, Fe/Fe₃O₄ and Fe₃O₄ nanoparticles was 21±3, 26±2 and 25±2 s. To clarify this divergence, the presence of dipole-dipole interactions incorporating a reversible aggregation-assisted separation should be considered. Such mechanism occurs when the Bjerrum length, the distance between particles with parallel dipoles at which the attractive magnetic energy becomes equal to the thermal energy, is larger than the particle diameter [9]. In the studied samples not only this condition is satisfied but the relatively large particle size and the increased concentration contribute in the acceleration of separation. The measured separation rates

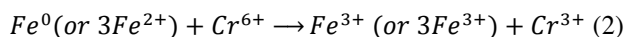
were found in agreement to the prediction of complete separation time t_s by the empirical equation for the reversible aggregation mechanism [9]:

$$t_s = t_0 \left[\left(\frac{3k_B T \rho}{2\mu_0 M_s^2 C} \right)^{1/3} \frac{2}{D} \right]^{0.73} \quad (1)$$

where t_0 is a time constant set at 66 s, D is the particle's diameter, M_s the saturation magnetization, k_B the Boltzmann's constant, μ_0 the magnetic permeability, T the temperature, ρ the particle density and C the dispersion concentration. More specifically, the separation time was calculated in the range 25-30 s for the three samples.

3.3 Cr(VI) uptake

The efficiency of the samples in the removal of Cr(VI) is described by the quantity of Cr(VI) captured by a mass of the nanoparticles for a specific residual concentration. The chromate removal isotherms measured at pH 7 and concentrations below 1 mg/L are also indicative for the applicability under reliable conditions, showing the potential of the nanoparticles to reduce Cr(VI) below the regulation limit. As shown in Figure 5, zero-valent iron nanoparticles are much more efficient compared to the magnetite ones, as expected according to the electron donation ability per iron atom even in the case of FeO formation in the surface. This is an indication that Cr(VI) removal mechanism is actually based on the reduction reaction which produces the insoluble Cr(III) state:



Chromate removal by Fe nanoparticles overcomes 3 μg Cr(VI)/mg at the current regulation limit (50 $\mu\text{g/L}$) as extracted by fitting experimental points by Langmuir's equation. Though, surface passivation occurring during the reduction of chromate onto Fe^0 and Fe_3O_4 particles limits further extend of removal activity. On the other hand, the partial inhibition of passivation may be the reason for the improved efficiency of the binary Fe/ Fe_3O_4 nanoparticle system compared to the single Fe_3O_4 nanoparticles, since that cannot be explained by the relatively low iron's content. A possible electron interaction in a supposed nanoscale galvanic element between Fe_3O_4 and Fe actually increases the lifetime of Fe_3O_4 nanoparticles in reducing chromate oxy-ions. Importantly, dissolved iron concentration in the treated water was found always below 0.1 mg/L.

4 Conclusions

Magnetic iron-based nanoparticles produced by Solar PVD were found adequate to remove hexavalent chromium below the current regulation limit for drinking water. Since reduction to the trivalent state is the occurring mechanism, the efficiency is defined by the composition of nanoparticles and the oxidation state of iron atoms setting ZVI nanoparticles the most advantageous for the treatment of chromium

contaminated water. In addition, the relative large size (45-80 nm) and the increased magnetization of the studied samples enable the easy application of a magnetic separation procedure.

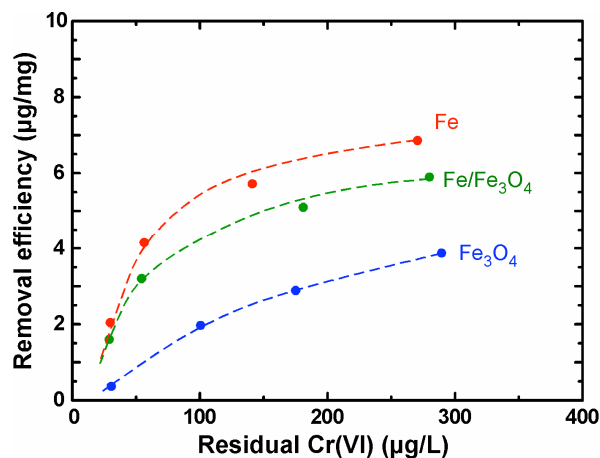


Fig. 5. Chromate removal isotherms at pH 7 for the Fe, Fe/ Fe_3O_4 and Fe_3O_4 nanoparticles. Dotted lines correspond to the Langmuir model's fitting of the points.

Acknowledgements

This work was supported by "Education and Lifelong Learning" Operational Program funded by EU-European Social Fund and Greek Secretariat for Research and Technology, the Spanish MEC (MAT2009-08024), CONSOLIDER (CSD2007-00041), and FEDER program. Financial support by the Access to Research Infrastructures activity in the 7th Framework Program of the EU (SFERA Grant Agreement n. 228296) is gratefully acknowledged. C.M. Boubeta thanks the "Ramón y Cajal" Spanish program.

References

1. J. Hu, I.M.C. Lo, G.H. Chen, Sep. Purif. Technol., **56**, 249 (2007)
2. D. Mohan, C.U. Pittman Jr., J. Hazard. Mat., **142**, 1 (2007)
3. S. Tresintsi, K. Simeonidis, G. Vourlias, G. Stavropoulos, M. Mitrakas, Wat. Res., 10.1016/j.watres.2012.06.049
4. C.D. Palmer, P.R. Wittbrodt, Environ. Health Perspect., **92**, 25 (1991)
5. European Council, Council Directive (98/83/EC), Offic. J. Eur. Commun., L330 (1998)
6. D. Mohan, C.U. Pittman Jr, J. Hazard. Mat., **B137**, 762 (2006)
7. C.J. Monty, Arab. J. Sci. Eng., **35**, 93 (2010).
8. K. Simeonidis, Th. Gkinis, S. Tresintsi, C. Martinez-Boubeta, G. Vourlias, I. Tsiaoussis, G. Stavropoulos, M. Mitrakas, M. Angelakeris, Chem. Eng. J., **168**, 1008 (2011)
9. G. De Las Cuevas, J. Faraudo, J. Camacho, J. Phys. Chem. C, **112**, 945 (2008)